Motion of a Floating Structure in Water of Uniform Depth

Jin S. Chung*
Lockheed Missiles and Space Company, Sunnyvale, Calif.

A potential flow theory is used to develop a method and an associated computer program that computes the hydrogynamic forces and six degrees-of-freedom motion for floating structures of general configuration at arbitrary heading in waves in water of uniform depth. The hydrodynamic force equation derived become identical, under certain assumptions, to the equations commonly used by the offshore industry, and the two approaches are compared in detail. The computed motions for all six degrees of freedom agree well with model-scale and full-scale experimental data for two typical semisubmersible drilling rigs in finite-depth water. Also, the present motion computations are more accurate than a prior work using the second approach; they use experimentally validated or determined values of hydrodynamic coefficients with the effect of the free surface and water depth included. The present method generates sufficient computation accuracy to use for practical design applications.

Nomenclature

A = incident wave amplitude
A_{cwi} = waterplane area of the ith column segment
A_{hwi} = waterplane area of the ith hull segment
A_{wpi} = $A_{cwi} + A_{hwi}$
A_{jk} = added-mass coefficients ($j,k = 1,2...6$)
B_{jk} = damping coefficients ($j,k = 1, 2...6$)
C_{jk} = restoring force coefficients ($j, k = 1, 2...6$)
C_d = drag coefficient
C_x = cross-sectional contour of the ith segment
F_j = exciting forces and moments ($j = 1, 2...6$)
H_i = wetted length of the ith column segment
I_j = rig moment of inertia in the jth mode ($j = 4, 5, 6$)
L_i = length of the ith hull segment
M = rig mass
N = total number of pairs of the column and hull segments
R_e = Reynolds number ($R_e = \ell \mid v_{ji}^r \mid / \nu$)
T = wave period, sec
T_n = natural period of motion
V_i = displaced-water volume of the ith segment
a = characteristic cross-sectional dimension of the segment
a_{jk} = segmental added-mass coefficients ($j, k = 1, 2, 3$)
b_{jk} = segmental wave-damping coefficients ($j, k = 1, 2, 3$)
b_{jj}^* = linearized drag coefficients
c = subscript to denote pertinence to column members
c_{jk} = segmental hydrostatic restoring coefficients ($j, k = 1, 2, 3$)
g = gravitational acceleration
h = water depth; also, as subscript, denotes the hull
k = wave number; $k_1 = k\cos\beta_i$; and $k_2 = k\sin\beta_i$
m_{ci} = displaced-water mass by the ith column segment
m_{hi} = displaced-water mass by the ith hull segment
m_i = either m_{ci} or m_{hi}
n_j = generalized normal ($j = 1,2,3$)
s_i = the ith segment surface
$v_j, \dot{v}_j$ = water-particle oscillatory velocity and acceleration for the jth mode
v_{ji}^r = relative velocity of the ith segment for the jth mode of motion
x_j = $x_i = x_1$, $y_i = x_2$, and $z_i = x_3$
x_L = length of the ith segment
z_{hi} = vertical distance of the hull segment axis below the c.g.
α = incident-wave direction relative to the x axis
β_i = incident-wave direction relative to the x_i axis
γ_i = angle between the x- and x_i-axes
ℓ = characteristic length
ξ, η, ζ = translatory dislacements of the rig c.g. and correspond to surge, sway and heave, respectively ($\chi_j, j = 1, 2, 3$)
ξ_i, η_i, ζ_i = displacements of the ith segment point in the x_i, y_i, and z_i directions, respectively
ϕ, θ, ψ = angular displacements about the rig c.g. and correspond to roll, pitch, and yaw, respectively ($\chi_j, j = 4,5,6$)
Φ = unsteady velocity potential
ϕ_I = amplitude of the incident-wave potential
ϕ_D = amplitude of the diffraction potential
ϕ_j = amplitude of the oscillatory potential
ρ = fluid density
χ_j = motion displacements in the jth mode ($j = 1, 2...6$)
χ_{ji} = the jth directional motion of the ith segment
ω = wave frequency in rad/sec
$\bar{\omega}$ = dimensionless frequency ($\bar{\omega} = \omega^2 a/g$)

I. Introduction

TWO approaches generally have been used for the hydrodynamic force equations for a floating, multihull platform in waves (Fig. 1). The "first" approach applies potential flow theory, which has been used commonly for the ship motion problem, and mathematically derives the "Froude-Krilov" force, the "diffraction" force, and the force due to the motion. Kim[1] applied it to a floating platform in water of infinite depth, without relating it to the "second" approach. His equations of motion include coupling between a pair of the three modes of motion: surge-heave-pitch and sway-roll-yaw. The "second" approach[2-8] is to use an approximate equation directly for the wave force and the force due to the motion, often without fully realizing restrictions on it; the wave force is the same as the well-known semiempirical method for the wave-induced inertia force plus drag force on a submerged body commonly used in the field of coastal engineering.[9] The hydrogynamic force equations,[2-8] which use the second approach, share major features and differ in some detail only, and the extent of coupling between the modes of motion differs in detail.

Motion computations for infinite depth reported in Refs. 2, 3, 7, and 8 neglected effects of the free surface on the hydrodynamic (added-mass and wave-damping) coefficients. Computations for finite depth[3,5] neglected the effects of the free surface and water depth on the hydrodynamic coef-

Received June 16, 1975; revision received Feb. 10, 1975.
Index categories; Hydrodynamics; Marine Hydrodynamics, Vessel and Control Surface; and Marine Vessel Design (including Loads).

*Research Specialist, Hydrodynamics Department, R&D Division. Member AIAA.

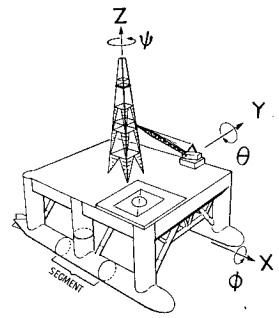

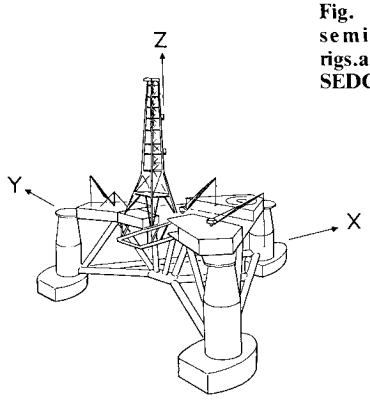

Fig. 1 Sketch of semisubmersible rigs.a) MOHOLE b) SEDCO 135-F.

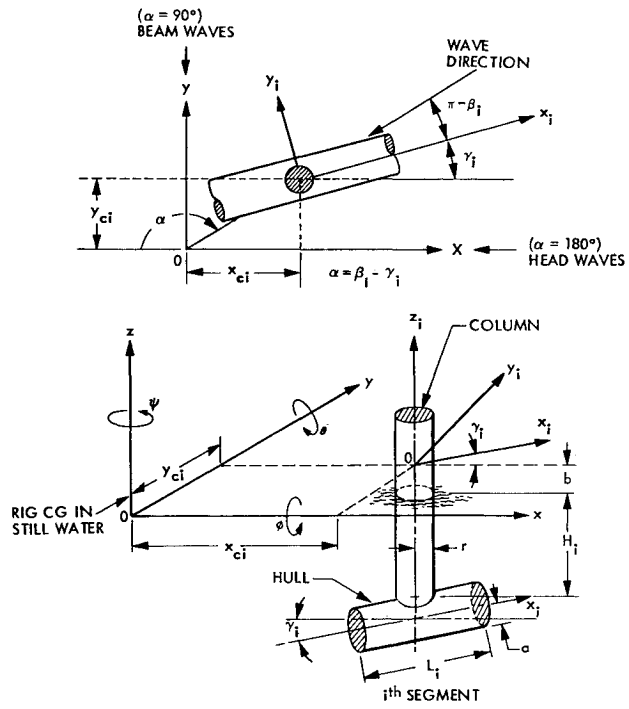

Fig. 2 The coordinate systems of the member segments.

ficients. The hydrodynamic coefficients of the individual structural members with the effects of the free surface and water depth are not presented in Refs. 2, 3, 5, 7, and 8; nor did Refs. 1 and 5-8 provide computations of all six degrees of motion. Authors of Refs. 2,5, and 7 did not compare the computed motions with any experimental data. Some force equations[1,2,7] handle only the limited structural-member arrangement; the structural members are parallel to each other. Also, Refs. 1-3, 5, 7, and 8 did not relate the results to operational practice.

The present expressions of the linearized hydrodynamic forces are derived[10] by the first approach, which uses a potential flow theory previously used for a ship-motion problem.[11] The equations are reduced with a few reasonable assumptions[10] to the same form as the equations used by the second approach, justifying a part of the second approach. The two approaches are compared in detail. For a structure of general configuration, the structural members can be arranged arbitrarily, and nearly all modes of motion are coupled. All coupled six degrees-of-freedom motion are computed for finite depth with hydrodynamic coefficients, which include the effects of a free surface and water depth. The motions computed for the "three-column-stabilized" SEDCO 135-F semisubmersible rig are compared with existing experimental data, model-scale[12] for all six-degrees-of-freedom motion and in full-scale[13] for heave only. Heave motion also is computed for the "six-column-stabilized" MOHOLE rig model.[2] The mathematical treatment and the interpretation of the results are related to operational practice. The present paper derives the equations of motion, the hydrodynamic force equations, and the hydrodynamic coefficients in the next three sections. Discussions on the numerical computation, the practical hydrodynamic-coefficient values, and the test of the method's validity follow with conclusions.

II. Formulation of Equations of Motion

A Cartesian body (x,y,z) coordinate system has its origin at the center of gravity (c.g.) of a floating structure with the undisturbed free surface at $(0,0,-b)$ (Fig. 2). The z axis is positive upward, perpendicular to the $x-y$ plane. The structural members are idealized as many continuous member segments, vertical and horizontal. The hydrodynamic treatment is made on each individual segment for the submerged portion of the structural members. A segment (x_i, y_i, z_i) coordinate system is introduced for the center of the ith segment volume and has its origin at a point $(x_{ci}, y_{ci}, 0)$. The z_i axis is vertical along the column-segment axis. The members parallel and normal to the undistrubed free surface are called a hull and a column, respectively.

The slopes of the incident waves are assumed to be small so that the waves may be described as infinitesimal. It is assumed that the oscillatory, rigid-body responses of the structure are linear and harmonic. The six, linear, coupled differential equations of motion can be written

$$\sum_{k=1}^{6} [\,(M_{jk}+A_{jk})\ddot{\chi}_k + B_{jk}\dot{\chi}_k + C_{jk}\chi_k\,] = F_j e^{i\omega t} \qquad (1)$$

where $\xi(t)=\chi_1$, $\eta(t)=\chi_2$, $\zeta(t)=\chi_3$, $\phi(t)=\chi_4$, $\theta(t)=\chi_5$, $\psi(t)=\chi_6$, and $j=1, 2...6$. M_{jk} are the components of the generalized mass matrix for the structure, A_{jk} and B_{jk} are the added mass coefficients and damping coefficients, respectively, C_{jk} are the hydrostatic restoring coefficients, and F_j are the exciting forces and moments. The dots stand for derivatives with respect to time, so that $\dot{\chi}_k$ and $\ddot{\chi}_k$ stand for velocity and acceleration, respectively, for the motion of the structure's c.g.

It is assumed that the structure is symmetric about the $x-z$ plane, and its c.g. is located at the origin of the body coordinate system. The nonzero components of M_{jk} are given by

$$M_{jj} = \begin{cases} M & \text{for } j=1,2,3 \\ I_4, I_5, I_6 & \text{for } j=4,5,6 \end{cases}$$

$$M_{46} = -I_{46} = -I_{64} \qquad (2)$$

where M is the mass of the structure, I_j is the moment of inertia in the jth mode, and I_{jk} is the product of inertia. I_{46} vanishes if the structure has fore-and-aft symmetry and is small otherwise; many recent drilling rigs have $I_{46}=0$. Other components vanish, since the origin of the body coordinate system is the same as the c.g. of the structure.

The nonzero added-mass (or damping; B_{jk}) coefficients for the structure in the body coordinate system are

$$A_{jj}\,(j=1,2...6) \qquad A_{21}\neq A_{12} \qquad A_{41}=A_{14} \qquad A_{51}=A_{15}$$

$$A_{61}=A_{16} \qquad A_{42}=A_{24} \qquad A_{52}=A_{25} \qquad A_{62}=A_{26}$$

$$A_{53}=A_{35} \qquad A_{64}=A_{46} \text{ and } A_{65}=A_{56} \tag{3}$$

For the stationary structures treated, $A_{jk}=A_{kj}$, and $B_{jk}=B_{kj}$. Unlike a monohull body,[11] A_{jk} and B_{jk} are additionally coupled between the modes of sway-surge, roll-surge, yaw-surge, pitch-sway, and yaw-pitch. The couplings for these coefficients exist for many floating structures with $\gamma_i \neq 0$. For the floating structures that are symmetric about the $x-z$ plane and $\gamma_i=0$, $A_{12}=A_{14}=A_{16}=A_{25}=A_{56}=0$, and similarly for the corresponding B_{jk}. The special case of $\gamma_i=0$ includes Refs. 1, 2, 6, 7, and 14 and Refs. 3 and 8 are not specific about γ_i.

The nonzero linear hydrostatic restoring coefficients for the structure in the body coordinate system are

$$C_{33}, C_{44}, C_{55}, \text{ and } C_{35}=C_{53} \tag{4}$$

A_{jk}, B_{jk}, C_{jk}, and F_j are derived later in detail. Equation (3) indicates coupling between nearly all six modes of motion. Therefore, all six equations of motion of Eq. (1) must be solved simultaneously.

III. Formulation of Hydrodynamic Force Equations

General Description

The total force on the submerged portion of a segment consists of: 1) Froude-Krilov force, the force from the pressure distribution due to the undisturbed waves acting on the segment in its mean position; 2) "diffraction" force, the force due to the waves disturbed by the presence of the segment in its mean position; 3) "motion-dependent" force, the force due to the motions of the segment oscillating rigidly with the structure; and 4) hydrostatic forces. The "wave force" consists of the Froude-Krilov force and the diffraction force, and the term "wave force" has been used commonly in the offshore industry to designate the exciting force. The total force described in the preceding is derived for finite depth, but also is applicable in infinite depth.

Mathematical Approach

The present derivation follows the procedure of the author of Ref. 10, which uses potential flow theory, and leads to the forms[2-9] of the force equations which followed the second approach. Similarities and difference between the two approaches have been shown.[10] The linearized velocity potential $\Phi(x, y, z; t)$ must satisfy the Laplace equation, the linearized boundary condition of the free surface, and the boundary condition of uniform depth. The boundary conditions on the free surface and of uniform depth give the relationship for finite depth, h,

$$\omega^2/g = k \tanh kh \tag{5}$$

Let the linearized velocity potential for zero speed of advance be

$$\Phi(x, y, z; t) = \phi_t(x, y, z)\, e^{i\omega t} \tag{6}$$

$$= (\phi_I + \phi_D + \sum_{j=1}^{3} \chi_j \phi_j)\, e^{i\omega t} \tag{7}$$

where ϕ_I is the incident-wave potential, ϕ_D is the diffraction potential, χ_j are the complex amplitudes of the motion, and ϕ_j are the oscillatory potential to the motion. The subscript j indicates the jth direction.

Additionally, the velocity potentials in Eq. (7) each should satisfy the appropriate boundary condition at infinity. Also, the linear bounary conditions on the segment surface at its mean position and in the jth mode of oscillation, respectively, must be satisfied,

$$(\partial\phi_I/\partial n) + (\partial\phi_D/\partial n) = 0 \tag{8}$$

$$\partial\phi_j/\partial n = i\omega n_j \tag{9}$$

The pressure distribution at the free surface may be taken to be zero; then the wave-surface elevation can be written

$$\tilde{\zeta}_i(x_i, y_i; t) = A\cos(k_1 x_i - k_2 y_i - \omega t) - \zeta_i(t) \tag{10}$$

where $\zeta_i(t) = \zeta + y_{ci}\phi - x_{ci}\theta$ is the total vertical displacement of the waterplane area of the ith segment. The subscript i denotes the ith segment. We shall stay in the segment (x_i, y_i, z_i) coordinate system until otherwise stated.

The subsurface pressure (for $z_i < \tilde{\zeta}$) on the ith segment point can be written

$$p_i = -\rho[g\{\zeta_i(t) + z_i\} + \dot{\Phi}(x_i, y_i, z_i; t)] \tag{11}$$

Integration of Eq. (11) over the ith segment surface gives

$$(X_j)_i e^{i\omega t} = -\rho \iint_{s_i} n_j (\dot{\Phi})_i ds_i \qquad j=1,2,3 \tag{12}$$

where s_i is the segment surface. The hydrostatic force term in Eq. (11), which is not included in Eq. (12), is reintroduced later.

By applying Eq. (7) to Eq. (12), the linear hydrodynamic force on the ith segment for the jth direction can be divided into three parts as

$$(X_j)_i = X_j^{F-K} + X_j^D + X_j^M \qquad j=1, 2, 3 \tag{13}$$

where

$$X_j^{F-K} = -i\rho\omega \iint_{s_i} n_j \phi_I ds_i \qquad \text{Froude-Krilov force} \tag{14}$$

$$X_j^D = -i\rho\omega \iint_{s_i} n_j \phi_D ds_i \qquad \text{diffraction force} \tag{15}$$

$$X_j^M = -i\rho\omega \iint_{s_i} n_j \sum_{k=1}^{3} \chi_k \phi_k ds_i \qquad \text{motion-dependent force} \tag{16}$$

The subscript i will be dropped, until otherwise stated, to indicate the ith segment. Indeed $(X_j^{F-K} + X_j^D)$ is the wave force.

Froude-Krilov Force

Φ_I in Eq. (6) can be defined for finite depth,

$$\Phi_I = \frac{igA}{\omega} \frac{\cosh k(z+h+b)}{\cosh kh} \exp[-i(k_1 x - k_2 y - \omega t)] \tag{17}$$

Applying Gauss' theorem to change the surface integral in Eq. (14) to the volume integral, Eq. (14) can be written

$$X_j^{F-K} e^{i\omega t} = \rho \iiint_{V_i} \dot{v}_j dV_i \tag{18}$$

Thr present derivation uses Eq. (18) to secure the Froude-Krilov forces, whereas Eq. (14) is used directly by Kim[1] for a floating structure for infinite depth and by Savesen, et al.[11] for ship motions. The water-particle orbital velocity and acceleration, respectively, at a point (x_i, y_i, z_i) with Eq. (17) are obtained

$$v_j = \partial\Phi_I/\partial x_j \text{ and } \dot{v}_j = \partial\dot{\Phi}_I/\partial x_j \tag{19}$$

Equation (19) must satisfy Eq. (5), from which k also can be obtained.

A few assumptions[10] are joined in evaluating Eq. (18) for the sake of making the computations simple and fast. The submerged portions of the members for the majority of the existing floating structures have cross-sectional dimensions, which are very small as compared to the wavelength. Consequently, it is assumed that the member consists of many segments, small compared to the wavelength and water depth, that the force may be taken as acting on the displaced-water volume centerlines of the segments, and that the motion of the wave surface is uniform across the cross-sectional surface of the segment about its waterplane center. The first assumption implies that $kx_i \ll 1$ and $ky_i \ll 1$ for the column segment, $ky_i \ll 1$ and $kz_i \ll 1$ for the hull segment, and $kh \geq O(1)$. Authors of Refs. 3, 5, and 8 failed to point out the assumption regarding to the water depth in treating bodies in finite depth.

Applying the preceding assumptions to Eq. (18) gives

$$X_j^{F-K} e^{i\omega t} = \rho A_i \int \dot{v}_j dx_L = (m_i/x_L) \int \dot{v}_j dx_L \tag{20}$$

where A_i is the cross-sectional area of the segment, $m_i = \rho A_i x_L$, dx_L is the length variable along the segment axis, and x_L is the segment length. The previous assumptions allow A_i and m_i to pass through the integral sign in Eq. (20), which makes the computations simple and fast. This also means that A_i is independent of x_L for the constant cross section C_x; the effect of the axial variation of the cross-sectional geometry of the member on the surrounding fluid is ignored. Substitution of Eq. (19) into Eq. (20) gives the Froude-Krilov force, which acts on the displaced-water volume centerline of the ith column and hull segments, respectively. The integration for the column segment should be carried out from $x_i = -L_i/2$ to $L_i/2$.

Without relating it to potential flow theory and the boundary conditions described previously, an equation that is essentially the same as Eq. (20) has been applied by others.[2-8] Equations (14) and (18) differ from Eq. (20) as a consequence of the preceding assumptions being applied to obtain Eq. (20) from (18). This procedure seems to have little affect on the computational accuracy, which is discussed later.

Diffraction Force

The incident waves are indeed disturbed by the presence of the segments, and this disturbance requires a correction to the Froude-Krilov force. This correction of the force will be called the diffraction force. The procedure[10] to secure the diffraction force is similar to that for Eq. (20).

Applying Eq. (9) to Eq. (15), and applying Green's second identity and Eq. (8) to it, respectively, give

$$X_j^D = -\rho \iint_{S_i} (\partial \phi_j / \partial n) \phi_D ds_i \tag{21}$$

$$= \rho \iint_{S_i} \phi_j (\partial \phi_I / \partial n) ds_i \qquad j = 1,2,3 \tag{22}$$

$ds_i = dx_L d\ell_i$, and $d\ell_i$ is element of the arc along C_x.

Applying to Eq. (22) the assumptions used to obtain Eq. (18) gives

$$X_j^D e^{i\omega t} = -\frac{1}{i\omega} \sum_{k=1}^{3} t_{jk} \int v_k dx_L \tag{23}$$

where

$$t_{kj} = -i\rho\omega \int_{C_x} n_k \phi_j d\ell_i \tag{24}$$

For a long slender member, $\partial/\partial x_i \ll \partial/\partial x_i \ll \partial/\partial z_i$ for the hull segment, and $\partial/\partial z_i \ll \partial/\partial x_i$ and $\partial/\partial z_i \ll \partial/\partial y_i$ for the column segment. Then ϕ_j can be assumed to be two dimensional; $j = 2,3$ for the hull segment and $j = 1,2$ for the column segment. Hence, Eq. (24) becomes

$$t_{jk} = \omega^2 a_{jk} - i\omega b_{jk} \qquad j,k = 1,2,3 \tag{25}$$

where a_{jk} and b_{jk} are two-dimensional added-mass coefficients and wave-damping coefficients per unit length of the segment. For the cylinder segment of constant C_x along x_L, $t_{jk} = 0$ for $j \neq k$; for the definition[5] of the coordinate axis for an arbitrary hull form, generally $a_{jk} \neq 0 \neq b_{jk}$, not $a_{jk} = 0 = b_{jk}$, as used in Ref. 5, when $j \neq k$.

Equations (23), with t_{jj}, can be expressed in terms of a_{jj} and b_{jj}:

$$X_j^D e^{i\omega t} = a_{jj} \int \dot{v}_j dx_L + b_{jj} \int v_j dx_L \tag{26}$$

Equation (26), with Eq. (19), can be expressed for the ith column and hull segments, respectively, in terms of the acceleration and velocity term. The integrand associated with $\dot{v}_j$ in Eq. (26) is exactly the same as the integrand of Eq. (20); Eq. (20) is associated with m_i, whereas Eq. (26) is associated with a_{jj} and b_{jj}. Equation (22) is more general than, and differs from, Eq. (26) because of the results due to the assumptions.

The wave force is the sum of Eqs. (20) and (26),

$$X_j^W e^{i\omega t} = (m_i/x_L + a_{jj}) \int \dot{v}_j dx_L + b_{jj} \int v_j dx_L \tag{27}$$

Equations (27) is essentially the same as the approximate wave-force equation used by the second approach without relating it to potential flow theory and the boundary conditions described previously. The second approach ignored the b_{jj}-term and does not relate X_j^D in Eq. (26) to the diffraction force.

Motion-Dependent Force

The motion-dependent forces are obtained as if the member segments undergo an oscillatory motion in still water with a free surface. Equation (16) together with Eq. (9), becomes

$$X_j^M e^{i\omega t} = \int t_{jj} \chi_{ji} dx_L \qquad j = 1,2,3 \tag{28}$$

The $x_{ji} = f(\chi_j)$ is the j-directional motion of the ith segment, is initially unknown, and can be computed by an iteration process from the computed motion χ_j of the structure. The iteration process is described in Sec. V. Accordingly, $\ddot{\chi}_{ji}$ and χ_{ji} can be computed.

Equations (28), together with Eq. (25) can be written in terms of a_{jj} and b_{jj}

$$X_j^M e^{i\omega t} = -x_L (a_{jj} \ddot{\chi}_{ji} + b_{jj} \dot{\chi}_{ji}) \tag{29}$$

Equation (29) is essentially the same as the equation forms used by the second approach. For the derivation of Eq. (29), it is assumed that the cross section of the segment does not vary along the segment axis. In the next section Eq. (13), obtained in terms of Eqs. (20, 26, and 29) in the segment (x_i, y_i, z_i) coordinate system for the ith segments, will be transformed to the body coordinates (x, y, z) for the entire floating structure.

Hydrodynamic Forces on the Floating Structure

The components of the hydrodynamic forces [Eq. (13)] derived in the segment coordinate system are found along the x, y, and z directions, and then are summed in the body coordinate system for all the column and hull segments. Equations (13) gives the hydrodynamic forces in the body coordinate system for the entire floating structure

$$X = \sum_{i}^{N} X_i' = \sum_{i=1}^{N} [(X_{ci} + X_{hi}) \cos\gamma_i - (Y_{ci} + Y_{hi}) \sin\gamma_i] \tag{30}$$

$$Y=\sum_{i}^{N} Y_i'=\sum_{i=1}^{N}\left[(Y_{ci}+Y_{hi})\cos\gamma_i+(X_{ci}+X_{hi})\sin\gamma_i\right] \quad (31)$$

$$Z=\sum_{i}^{N} Z_i'=\sum_{i=1}^{N}(Z_{ci}+Z_{hi}) \quad (32)$$

where N is the total number of pairs of the column and hull segments, and $X_i=(X_1)_i$, $Y_i=(X_2)_i$, and $Z_i=(X_3)_i$. The subscript "c" stands for a column and the subscript "h" for a hull.

Equation (13) on the indivdual segments can be used as the hydrodynamic force distributions along the structural members. For fine distributions of the hydrodynamic forces, the computations can be made for as many segments for the given members as desired within the framework of the theory and assumptions involved. The force distributions are essential information for the structural analysis. Note that the possible hydrodynamic coupling between members are ignored. On the other hand, the hydrodynamic forces in Eqs. (30-32) can be used for the equations of motion from which A_{jk}, B_{jk}, C_{jk}, and F_j will be derived in the body coordinate system.

IV. Coefficients and Exciting Forces and Moments

Equations of Motion

The linearized equations of motion in the body coordinate system for a floating structure are as follows:

$$M\ddot{\xi}=X \quad (33)$$

$$M\ddot{\eta}=Y \quad (34)$$

$$M\ddot{\zeta}=Z-\rho g\sum_{i=1}^{N} A_{wpi}\zeta_i \quad (35)$$

$$I_4\ddot{\phi}=\sum_{i=1}^{N}\left[-\int_{H_i}\left(\frac{d}{dz}Y_{ci}'\right)z\,dz+Y_{hi}'z_{hi}+Z_i'y_{ci}+g(m_{hi}z_{hi}-m_{ci}z_1)\phi\right] \quad (36)$$

$$I_5\ddot{\theta}=\sum_{i=1}^{N}\left[\int_{H_i}\left(\frac{d}{dz}X_{ci}'\right)z\,dz-X_{hi}'z_{hi}-Z_{ci}x_{ci}-\int_{L_i}\left(\frac{d}{dx}Z_{hi}\right)x\,dx+g(m_{hi}z_{hi}-m_{ci}z_1)\theta\right] \quad (37)$$

$$I_6\ddot{\psi}=\sum_{i=1}^{N}\left[-X_i'y_{ci}+Y_{ci}'x_{ci}+\int_{L_i}\left(\frac{d}{dx}Y_{hi}'\right)x\,dx\right] \quad (38)$$

where

$$z_1=\frac{1}{H_i}\int_{-(H_i+b)}^{-b} z_i\,dz_i$$

$$A_{wpi}=A_{cwi}+A_{hwi}$$

and

$X_i'=(X_{ci}'+X_{hi}')$ and $Y_i'=(Y_{ci}'+Y_{hi}')$ can be found from Eqs. (30) and (31).

A_{jk}, B_{jk}, C_{jk}, and F_j

Substituting Eqs. (30-32) into Eqs. (33-38), and grouping them in terms of $\ddot{\chi}_j$, $\dot{\chi}_j$, and χ_j ($j=1, 2...6$), respectively, before performing the summations give a_{jk}', $\bar{b}_{jk}'$, c_{jk}', and f_j' in the body coordinate system for the individual segments; j, $k=1,2...6$. The a_{jk}', $\bar{b}_{jk}'$, c_{jk}', and f_j' are the same as the segmental values, a_{jk}, $\bar{b}_{jk}$, c_{jk}, and $f_i, j, k=1,2,3$ in the segment coordinate system found in the segmental values in the body coordinate system, and additionally include coupling coefficients and exciting moments ($j,k=4,5,6$). It is noted that $c_{jk}'=c_{jk}$, and for $j=1,2,3$, $a_{jj}'=a_{jj}$ and $\bar{b}_{jj}'=\bar{b}_{jj}$.

Summations of a_{jk}', $\bar{b}_{jk}$, c_{jk}, and f_j' give A_{jk}, B_{jk}, C_{jk}, and F_j, defined in the body coordinate system for the entire structure

$$A_{jk}=\sum_{i=1}^{N} a_{jk}' \qquad B_{jk}=\sum_{i=1}^{N}\bar{b}_{jk}'$$

$$C_{jk}=\sum_{i=1}^{N} c_{jk}$$

$$F_j=\sum_{i=1}^{N} f_j' \quad (39)$$

for j, $k=1$, 2...6. The coefficients, a_{jk}, b_{jk}, and c_{jk} are discussed further later.

For Eqs. (30-32), a_{jj} and b_{jj} are already summed for a pair of the individual column and hull segments. This summation assumes that the possible hydrodynamic interference effect at the point of the column and hull intersection is small and can be ignored. Also, it is assumed that the possible hydrodynamic interferences between the hull segments or the column segments can be ignored. For many existing semisubmersible-like floating structures, the distance between the hulls or columns are so far that the hydrodynamic interferences between them can be ignored.

$$C_{33}=\rho g\sum_{i=1}^{N} A_{wpi} \qquad C_{35}=C_{53}=-\rho g\sum_{i=1}^{N} x_{ci}A_{wpi}$$

$$C_{44}=g\sum_{i=1}^{N}(\rho y_{ci}^2A_{wpi}+m_{ci}z_1-m_{hi}z_{hi})$$

$$C_{55}=g\sum_{i=1}^{N}(\rho x_{ci}^2A_{wpi}+m_{ci}z_1-m_{hi}z_{hi}) \quad (40)$$

For example, for the drilling operational mode of the semisubmersible rigs, $A_{hwi}=0$. C_{44} and C_{55} also can be expressed in terms of metacentric heights.

V. Numerical Computations

The six degrees-of-freedom motions are computed by solving Eq. (1) simultaneously for finite depth for two typical semisubmersible drilling rigs: MOHOLE and SEDCO 135-F (Fig. 1). The present computations use the hydrodynamic coefficients which include the effects of the free surface and water depth. Usually, wave components of $5<T<15$ sec are of interest for the drilling operations at sea, wave components of $T>15$ sec are of great interest for survival conditions in rough seas, and wave components of $T>25$ sec are rare. For a majority of the existing semisubmersible rigs, including the present two rigs, only the heave has its natural period at $T_n<25$ sec, and is the most important mode of motion in design and operation.

Added Mass and Wave Damping of a Segment

For the present motion computations of the member segments of MOHOLE rig, the author shall use Frank's theoretical method[16] and limited experimental data[4] for a_{jj} and b_{jj} (Fig. 3). For the case of SEDCO 135-F rig, actual hydrodynamic coefficients (Fig. 4) measured by a planar-motion-mechanism test[4] are used in the computations of the motion. Existing theoretical methods[16,17] can not compute the hydrodynamic coefficients accurately with the possible hydrodynamic interferences at the joints of the column segment with the hull segment (Fig. 1a), and at the joints of the oval footing with a column (Fig. 1b). Others [2-8] have treated the segments (e.g., MOHOLE) as two-dimensional

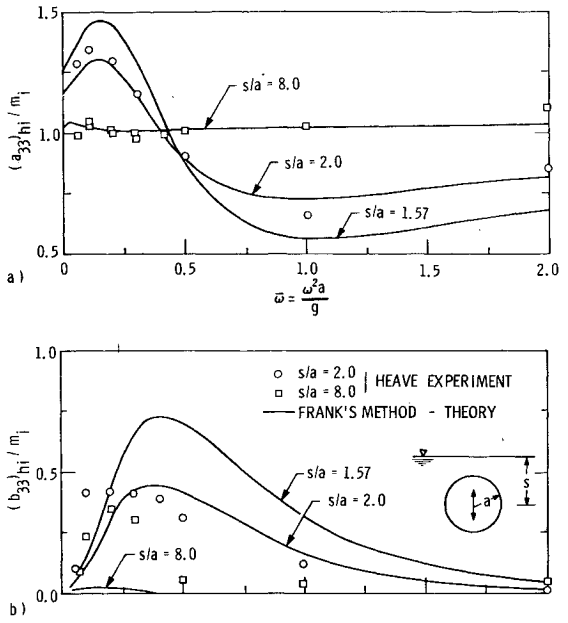

Fig. 3 a) Added-mass coefficients for a horizontal circular cylinder below a free surface ($h=\infty$); b) wave-damping coefficients

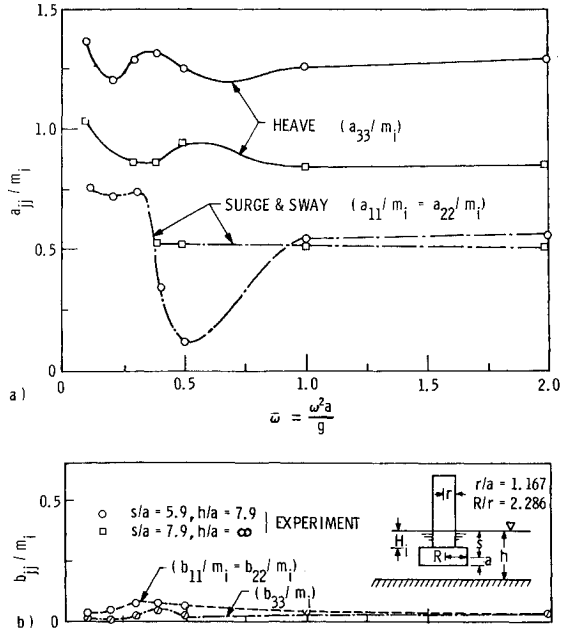

Fig. 4 a)Added-mass coefficients for a model of submerged oval with surface-piercing vertical circular cylinder; b) wave-damping coefficients.

and assumed no hydrodynamic interferences at the joints. These papers[2,3,5-8] further assumed no free-surface effect on a_{jj} and neglected b_{jj}. The oval footing with a vertical column (e.g., SEDCO 135 series) produces three-dimensional flow for the oval footing itself, and also at the joint of the oval footing with a column. In addition, very few experimental, hydrodynamic coefficient data have been published for the submerged segments under the influence of the free surface, or water depth, or both.

For the added mass and wave damping of a submerged hull segment oscillating near the free surface, the oscillation frequency range of interest for the main segment sizes of the majority of the semisubmersible rigs can be roughly $0.025 < \bar{\omega} < 1.0$ (or $5 < T < 25$ sec). As the submergence ratio s/a becomes smaller, the free-surface effect gets stronger over the $\bar{\omega}$-range. For small values of s/a, a_{jj} and b_{jj} for a cylinder can be different for the different directions of oscillations. For the segments of different cross-sectional geometries a_{jj} and b_{jj} are different. For finite-depth water with a free surface, the a_{jj} and b_{jj} (Fig. 4) generally get larger over the $\bar{\omega}$ range of interest, with an increase of $\bar{\omega}$ at the higher $\bar{\omega}$ range, as compared to the case of infinite fluid bounded by a free surface only.

Circular Cylinder for Infinite Depth

The MOHOLE rig consists of many segments of circular cross section (Fig. 3). For a hull segment,

$$(a_{11})_{hi} \approx 0 \quad (a_{22})_{hi} \approx (a_{33})_{hi},$$

$$(b_{11})_{hi} \approx 0 \quad (b_{22})_{hi} \approx (b_{33})_{hi}$$

For a surface-piercing column segment,

$$(a_{33})_{ci} \approx 0 \qquad (a_{11})_{ci} = (a_{22})_{ci},$$

$$(b_{33})_{ci} \approx 0 \qquad (b_{11})_{ci} = (b_{22})_{ci}$$

For a surface-piercing circular column[15] $(a_{11})_{ci} \approx 1.0 \approx (a_{22})_{ci}$, if the column diameter is small as compared with its length. This is also partially supported by an experimental results obtained for the model in Fig. 4, which shows that $a_{11} = a_{22}$ are practically independent of $\bar{\omega}$ for $s/a = 8$ ($H_i/r = 6$) and $h/a = \infty$ (Fig. 4a) where h/a is the finite-depth ratio, and that $b_{11} = b_{22}$ are small (Fig. 4b).

Figure 3 shows the heave ($j=3$) coefficients, which are determined for a submerged model of a horizontal, two-dimensional circular cylinder in water of infinte depth (40 times the radius of 11.43 cm for the planar-motion-mechanism experiment[4] with linear oscillation amplitudes) below the free surface. The experimental values of b_{jj} for $s/a = 2$ are obtained by subtracting the total damping coefficients obtained for $s/a = 8$ from total damping coefficients obtained for $s/a = 2$. The measured total damping coefficients for $s/a = 8$ are small and nearly a constant. Comparison of the theoretical computation[16] with limited experimental points[4] for $s/a = 2$ shows a good agreement, except for b_{jj}. The value of $\bar{\omega}$ for the measured maximum value of b_{jj} is lower than the corresponding $\bar{\omega}$ computed. The author's first-hand information indicates that the experiment showed little difference between the measured coefficients for the $s/a = 2$, $h/a = 8$ and the $s/a = 2$, $h/a = \infty$, and that the free-surface effect can be ignored for $s/a \geq 6$ and $h/a = \infty$.

For the MOHOLE rig, the drilling draft ranges from 18.3 to 21.3 m, corresponding to $2.43 \lesssim s/a \lesssim 3.0$, and the survival draft is 13.7 m, corresponding to $s/a = 1.57$. The water depth for the present calculation is $h = 61$ m, which corresponds to $h/a = 533.7$, and for the 21.3-m draft, $s/a = 3$. Thus, the water-depth effect on the coefficients is ignored for the reason stated previously, and only the free-surface effect is considered in the motion computation. The variation of the coefficients due to the free-surface effect is the greatest within the ω-range of practical interest.

Oval Footing with a Circular Cylinder

The SEDCO 135-series consists of three oval footings each with a vertical circular cylinder (Fig. 4) for which the hydrodynamic coefficients are three dimensional. Figure 4 shows the hydrodynamic coefficients expressed as a_{jj} and b_{jj} (although not two dimensional) for a model of a submerged oval footing with a vertical circular cylinder of 11.43 cm radius, which are determined by the planar-motion-mechanism experiment[4] for two water depths. For Fig. 4, $a_{jj} = (a_{jj})_{ci} + (a_{jj})_{hi}$ and $b_{jj} = (b_{jj})_{ci} + (b_{jj})_{hi}$, for $j = 1,2,3$; $a_{11} = a_{22}$ and $b_{11} = b_{22}$. These coefficients include the three-dimensional effect of the footing and the hydrodynamic interference effect at the joint. For $s/a = 6$ and $h/a = 8$, the free-surface effect on a_{jj}, although small, appears at the lower $\bar{\omega}$-range for a_{33}, but is significantly large for $a_{11} = a_{22}$ (Fig. 4a). For $s/a = 8$ and $h/a = \infty$, the free-surface effect slightly in-

fluences a_{33} at the lower $\bar{\omega}$ range, and has little practical effect on $a_{11}=a_{22}$; a_{33} is larger over the $\bar{\omega}$ range, and $a_{11}=a_{22}$ are only slightly larger at the higher $\bar{\omega}$ range for $h/a=8$ than for $h/a=\infty$. Figure 4b shows negligible small values of b_{jj}, which are obtained by the same procedure of eliminating the viscous damping as for the circular cylinder.

Motion computations of the SEDCO 135-F rig used the 24.4-m drilling draft, which corresponds to $s/a=5.4$, and the 37-m water depth, which corresponds to $h/a=8$. The footing of the SEDCO 135-F is slightly different from the oval footing, and can be expected to be very close to it in its hydrodynamic characteristics.

Viscous Damping

The damping of the segments consists of the wave damping and linearized viscous damping on the ith segment for the jth mode of oscillation

$$\bar{b}_{jj}=b^*_{jj}+b_{jj} \qquad b^*_{jj}=(8/3\pi)(\rho/2)C_dS_{ji}|v^r_{ji}| \qquad (41)$$

where b^*_{jj} is a linearized drag equivalent to a quadratic drag, C_d is a quadratic drag coefficient on the segment, and S_{ji} is a principal projected area of the ith segment. In order to utilize the linear motions theory, the quadratic drag is linearized as b^*_{jj}, following a method proposed in Ref. 18. It generates the factor $8/3\pi$. The jth directional oscillatory velocity of the ith segment relative to the water-particle velocity at the segment point is defined as,

$$v^r_{ji}=\int v_{ji}dx_L-\dot{\chi}_{ji} \qquad (42)$$

For a given Reynolds number R_e, b^*_{jj} can be obtained in terms of C_d; b^*_{jj} does not depend on the free-surface effect.

Present Motion Computations

The two semisubmersible rigs have different configuration and arrangement of the rig members. The MOHOLE rig has parallel hulls ($\gamma_i=0$) and a fore-and-aft symmetry for the computations; $A_{12}=a_{14}=A_{16}=A_{25}=A_{56}=A_{35}=0=B_{12}=B_{14}=B_{16}=B_{25}=B_{56}=B_{35}$. The geometric and other characteristics of the MOHOLE rig are estimated from Refs. 2 and 6. The characteristics of the SEDCO 135-F rig are those used for the model test:[12] the theory may not apply exactly to the footing, which is three dimensional. But the motion computations with a_{jj} and b_{jj} in Fig. 4 agree well with the model test data. Equations (1) are solved simultaneously. The present computations use the frequency-dependent values of a_{jj} and b_{jj} (Figs. 3 and 4). The a_{jj} values can influence the heave T_n significantly. Both b_{jj} and b^*_{jj} are taken into account, and $A=4.572$ m is used for the computation; v^r_{ji} also is a function of A through v_{ji} and χ_{ji}.

For the motion computations, C_d in Eq. (41) is selected initially from the wind-tunnel test data for a given segment geometry; v^r_{ji} is initially unknown, and the computations with the initially selected C_d use v^r_{ji} with $\dot{\chi}_{ji}=0$. For the second time, with the initially computed $\dot{\chi}_{ji}$, the resulting v^r_{ji} is used to compute the motions again. Then, the third time, a new v^r_{ji} is used. This iteration process for the given C_d is continued until the computed motions converge for all modes: except near T_n, the computed motions converge very fast. When the resonance amplitude of the final converged motion was larger than the model test data, the value of C_d was increased, the preceding iteration was repeated, and vice versa. Motions computed for a few additional semisubmersible rigs, not reported here, also have been tested. The results for all of the rigs show $C_d\approx 1.0$ for the segment. For the drilling drafts, the b^*_{jj} effect on the motion near T_n is dominant over b_{jj}. Since v^r_{ji} is a function of A, the larger the value of A, the smaller the transfer function near T_n, and vice versa.

Other Motion Computations

Previous papers[3,5] used the second approach for the motion computations for finite depth: the six degrees of motion for the SEDCO 135-F rig,[3] and only the heave, pitch, and yaw motions for the "STAFLO"rig.[5] Both computations[3,5] used constant-value a_{jj}, neglecting b_{jj} and the effects of the free surface and water depth on a_{jj}; v^r_{ji} was guessed at for the damping force.[3] The computed motions[5] for the latter rig were not compared with any experimental data.

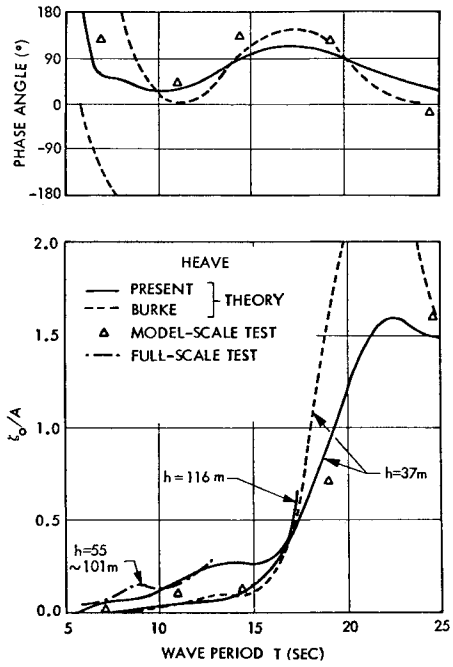

Fig. 5 Comparison of SEDCO 135-F heave computations with the model-scale and full-scale test data (waves 30°off bow).

Experimental Motion Data

The model test data[12] of motion amplitudes and phase angles (ϵ_j) for the SEDCO 135-F rig were obtained for regular waves; $h=37$ m, and the drilling draft was 24.4 m. For the full-scale test data[13] of motion amplitudes (no phase angles analyzed) for the SEDCO 135-F rig, the wave heading (α) was not known, and $h=55\sim 101$ m. Because of the uncertainty in the accuracy of the full-scale data for modes of motions other than heave, only the heave (Fig. 5), which is not substantially sensitive to the variation of α, is used for the present motion correlation. For the MOHOLE rig, the model test data[6] are obtained for "deep" water; h is claimed to be infinite, the draft is 21.3 m, and there are no model test data for finite depth.

The motion transfer functions presented in Figs. 5-11 are the steady-state values, $(\chi_j)_o/A$ from the expression $\chi_j/A=(\chi_j)_o/A\cos(\omega t-\epsilon_j)$ for $j=1, 2...6$, ϵ_j are positive when motions lag waves, with the wave crest being at the rig c.g. as a reference.

Motion Comparisons

Figure 5 shows, for the SEDCO 135-F rig, that the present heave computation for $h=37$ m agrees well over the T-range with the model-scale test data.[12] Heave also is computed for $h=116$ m, since the full-scale data were measured for the various water depths. The full-scale data[13] fall within the heave curves computed for the two depths. Note that Ref. 13 does not show data outside the T-range indicated in Fig. 5. Figure 5 also shows that the present heave computation is more accurate for both amplitude and phase angle than the other computations.[3] Both the model-scale test data and the present computation show $T_n\approx 22$ sec for heave. Since the member surface of the full-scale rig is rougher because of marine fouling than that of the scaled model, b^*_{jj} is expected to be larger and the heave amplitude near T_n is expected to be smaller in full-scale.

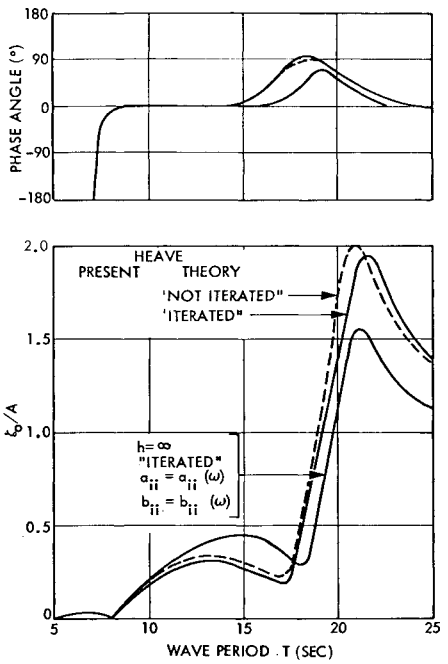

Fig. 6 Heave of MOHOLE (head waves; and $h = 61$ m and ∞).

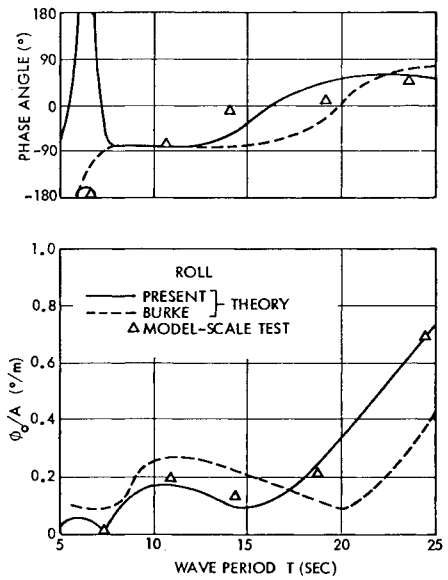

Fig. 7 Roll of SEDCO 135-F (beam waves; and $h = 37$ m).

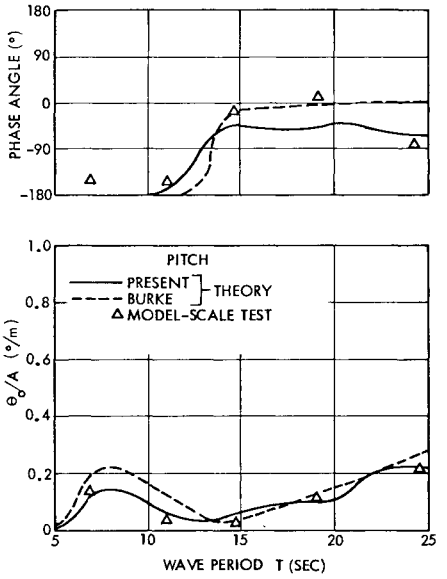

Fig. 8 Pitch of SEDCO 135-F (beam waves; and $h = 37$ m).

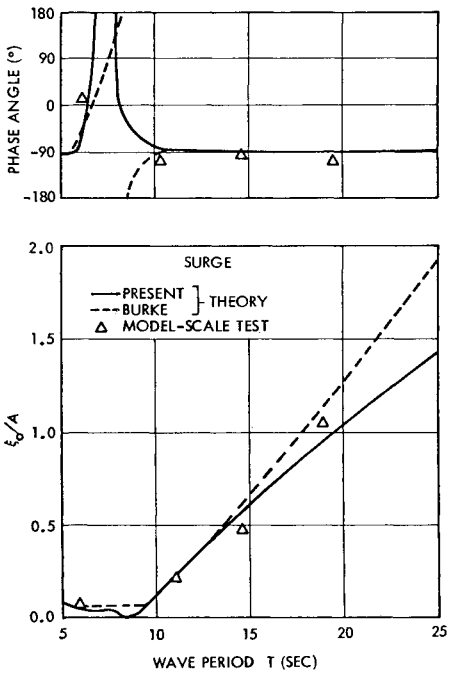

Fig. 9 Surge of SEDCO 135-F (waves 30°off bow; and $h = 37$ m).

Figure 6 shows the heave predictions for the MOHOLE rig for $h = 61$ m and ∞. The case of $h = \infty$ [4] shows that the prediction[4] agrees well with the model test data.[6] Figures 5 and 6 show that the heave amplitudes generally are smaller for finite depth up to $T \approx 18$ sec than for infinite depth, and that the heave T_n is longer for finite depth than for infinite depth. For finite depth, two heave curves are shown: one is a final value after the iteration described previously of the v_{ji}^r, and the other is the heave calculated with $\dot{\chi}_{ji} = 0$.

The present roll (Fig. 7) and pitch (Fig. 8) predictions for the SEDCO 135-F rig give good agreement in both the amplitudes and phase angles with the model-scale test data and clearly show better accuracy of roll predicitions over the other's.[3] Notice that Fig. 8 shows nonzero pitch for beam waves. This is because this rig has three pairs of semisubmerged columns and submerged footings, which are not symmetric about the y axis when the incident waves act on the submerged portion of the rig members. For the semisubmersible rigs with a symmetry about both the x and y axes, roll and pitch are zero for the head and beam waves, respectively. Surge (Fig. 9) and sway (Fig. 10) predictions for the SEDCO 135-F rig agree well with the model-scale test data. Unlike the surge and sway of ships, the surge amplitude in head waves and sway amplitude in beam waves are nearly the same for the present and other similar rigs. For yaw motions, comparison of the present computation with the scale-model test for the SEDCO 135-F rig gives good agreement in both the amplitude and phase angle (Fig. 11). Figure 11 also shows that the present prediction accuracy of yaw is better than the others.[3].

For the modes of motion other than heave, which has T_n within the T range of interest, the effects of a_{jj} and b_{jj} on motions are very small. This is because a_{jj} and b_{jj} influence the motion significantly only near its T_n, and except for heave the resonances occur at $T_n > 25$ sec, which has little practical significance.

VI. Conclusions

The well-known, semiempirical force equations are shown to be related to a general equation [Eq. (13)] derived from potential flow theory. The general equation is reduced to an

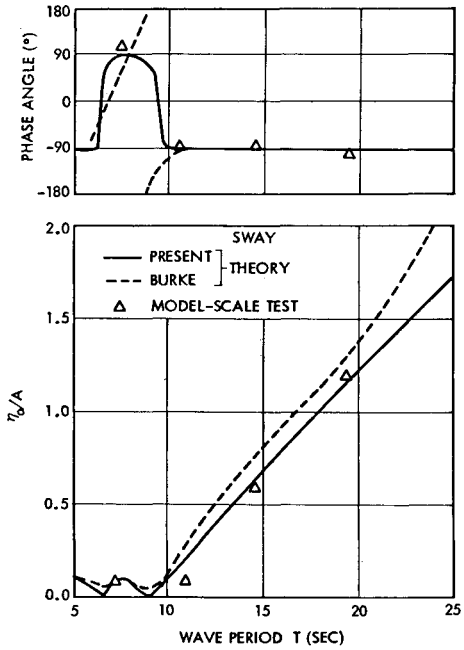

Fig. 10 Sway of SEDCO 135-F (beam waves; and $h = 37$ m).

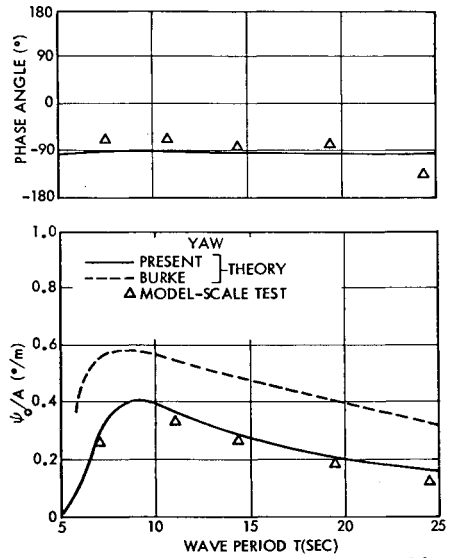

Fig. 11 Yaw of SEDCO 135-F (beam waves; and $h = 37$ m).

approximate equation, which is more complete than the semiempirical equations. The present derivations partly justify the semiempirical equations, producing additional terms for the approximate equation; the diffraction and motion-dependent forces with the effects of wave damping, and free surface and the damping force with the relative velocity.

The assumptions and the boundary conditions applied to the approximate equation can be validity and limitations imposed on the use of the present and semiempirical equations. The approximate equation makes the computations simpler and faster than the general equation, predicts motions that agree with the experimental data better than that of the others, which used the semiempirical equation, and generates sufficient computation accuracy for the motion predictions. Although it has been tested for motion predictions, it still appears to be important to use accurate values of the added-mass and damping coefficients for force computations.

References

[1] Kim, C.H. and Chou, F., "Motions of a Semi-Submersible Drilling Platform in Head Seas," Davidson Laboratory Rept., OE 71-8, Dec. 1971.

[2] Bain, J.A., "Extension of MOHOLE Platform Force and Motion Studies," Project MOHOLE Report, General Electric Co., Oct. 1964.

[3] Burke, B.G., "The Analysis of Motions of Semisubmersible Drilling Vessels in Waves," Paper 1024, *Proceedings of the Offshore Technology Conference*, Houston, Texas, April 1969.

[4] Chung, J.S., "Motions of Semisubmersible Drilling Rigs in Deep Water," *Journal of the Society of Naval Architects of Korea*, Vol. 11, 1974, pp. 23-40.

[5] Hooft, J.P., "A Mathematical Method of Determing Hydrodynamically Induced Forces on a Semi-Submersible," *Transactions of the Society of Naval Architects and Marine Engineers*, Vol. 79, New York, 1971, pp. 28-70.

[6] McClure, A.C., "Development of the Project MOHOLE Drilling Platform," *Transactions of the Society of Naval Architects and marine Engineers*, 1965, pp. 50-99.

[7] Ochi, M.K. and Vuolo, R.M., "Seakeeping Characteristics of Mult-Unit Ocean Platform," Presented at the Spring Meeting of the Society of Naval Architects and Merine Engineers, Honolulu, Hawaii, May 25-28, 1971.

[8] Paulling, J.R., "Elastic Response of Stable Platform Structures to Wave Loading," Proceedings of the International Symposium on the Dynamics of Marine Vehicles and Structures in Waves, Institute of Mechanical Engineers, London, Apr. 1-5, 1974, pp. 263-272.

[9] Wiegel, R.L., *Oceanographical Engineering*, Prentice-Hall, Englewood, Cliffs, N.J. 1964, p. 254.

[10] Chung, J.S., "A Note on the Two Force Equations for a Floating Platform," *Journal of Hydronautics*, Vol. 9, Oct. 1975, pp. 170-172.

[11] Salvesen, N., Tuck, E.O., and Faltinson, O., "Ship Motions and Loads," *Transactions of the Society of Naval Architects and Marine Engineers*, Vol. 78, New York, 1970, pp. 250-287.

[12] Van de Voorde, C.B. and Lap, A.J. W., "Model Tests for the SEDCO-Floating Drilling Platform," The Netherlands Ship Model Basin, Wageningen.

[13] Watts, J.S. et al., "A Performance Review of the SEDCO 135-F Semisubmersible Drilling Vessel," *Proceedings of Petroluem Society of CIM*, Calgary, Canada, May 1968.

[14] St. Dennis, M., "On the Motions of Oceanic Platforms," Proceedings of the International Symposium on the Dynamics of Marine Vehicles and Structures in Waves, Institute of Mechanical Engineers, London, Apr. 1-5, 1974, pp. 121-142.

[15] Mercier, J.A., "Hydrodynamic Forces on Some Float Forms," *Journal of Hydronautics*, Vol. 5, Oct. 1971, pp. 109-117.

[16] Frank, W., "Oscillation of Cylinder in or below the Free Surface of Deep Fluids," Department of the Navy, Washington, D.C., NSRDC Rept. 2357, 1967.

[17] Yamamoto, Y., "On the Oscillating Body under the Water Surface," *Journal of Zosen Kyokai*, Vol. 77, 1955, pp.29-41.

[18] Blagoveshchensky, S.N., *Theory of Ship Motion*, Dover, New York, 1962, pp. 140-142.